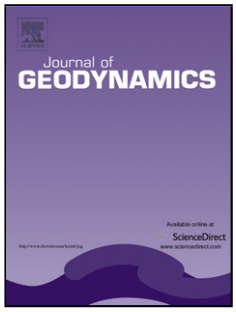

Title: Receiver function imaging of mantle transition zone discontinuities and the origin of volcanism beneath Libya

Authors: Awad A. Lemnifi, John Browning, Abdelsalam Elshaafi, Nassib S. Aouad, Y. Yu

PII: S0264-3707(18)30221-7
DOI: https://doi.org/10.1016/j.jog.2019.01.009
Reference: GEOD 1617

To appear in: *Journal of Geodynamics*

Received date: 8 September 2018
Revised date: 9 December 2018
Accepted date: 9 January 2019

Please cite this article as: Lemnifi AA, Browning J, Elshaafi A, Aouad NS, Yu Y, Receiver function imaging of mantle transition zone discontinuities and the origin of volcanism beneath Libya, *Journal of Geodynamics* (2019), https://doi.org/10.1016/j.jog.2019.01.009

Receiver function imaging of mantle transition zone discontinuities and the origin of volcanism beneath Libya

Awad A. Lemnifi[1, 2], John Browning[3], Abdelsalam Elshaafi[2], Nassib S. Aouad[1] , Y. Yu[4],

[1]Mining Engineering department, Missouri University of Science and Technology, Rolla, Missouri 65409, USA,

[2]Department of Earth Sciences, Faculty of Sciences, Benghazi University, Libya,

[3]Department of Mining Engineering and Department of Structural and Geotechnical Engineering, Pontificia Universidad Católica de Chile, Santiago, Chile

[4]State Key Laboratory of Marine Geology, Tongji University, Shanghai 200092, China

Abstract

The origin of magma at Libya's volcanic provinces is still poorly understood. In order to constrain these sources we report results of the first P-to-S receiver function investigation of the 410 km and 660 km depth discontinuities bounding the mantle transition zone (MTZ) beneath Libya. The dataset used by this study is a combination of eighteen seismic stations belonging to the Libyan Center for Remote Sensing and Space Science and the Incorporated Research Institutions for Seismology Data Management Center. The average thickness of the MTZ is found to be 249±14

km, which is similar to the global average. A 10 km thinning of the MTZ was observed beneath the Miocene – Holocene volcanic provinces in central Libya, suggesting higher-than-normal temperatures in those parts of the MTZ. Our preferred model suggests that the origin of volcanism in Libya is due to higher temperatures in the MTZ beneath this region. However, in Eastern Libya, the thickness of the MTZ increases from 249 km to 270 km which indicates a colder-than-normal MTZ which may relate to ancient subducted slabs due to the Africa-Europe convergence since the late Mesozoic.

Keywords: Mantle Transition Zone; Receiver functions; Libya; Seismic imaging; Volcanism

1. Introduction

Libya has experienced a complex tectonic history comprised by the development of a subduction zone in its northern-most portion [Capitanio et al., 2009; Faccenna et al., 2014; Lemnifi et al., 2015; 2017a], N-S and NW-SE oriented basement faults from the Pan-African Orogeny, and Hercynian compressional basement faults, which are also mainly orientated N-S or NW-SE [Hassan and Kendall, 2014; Lemnifi et al., 2015]. The region also hosts many volcanic provinces that were formed from the Miocene to the Holocene [e.g., Hoernle et al., 1995; Bardintzeff et al., 2012, Elshaafi and Gudmundsson, 2017] (Figure 1). These volcanic provinces are thought to be related to reactivation of pre-existing regional structures as a result of lithospheric stretching and astherospheric upwelling. These reactivations were in response to convergence between the African and European plates since the early Cretaceous [Beccaluva et al., 2007; Montagner et al.,

2007; Meert and Lieberman, 2008; Cvetkovi´c et al., 2010; Bardintzeff et al., 2012; Elshaafi and Gudmundsson, 2016, 2018; Lemnifi et al., 2017b].

The study of mantle discontinuities beneath Libya and adjacent regions are relatively sparse. This is partly due to the limited number of broadband seismic stations deployed in the area. Van der Meijde et al. [2005] studied seismic discontinuities in the Mediterranean region using P-to-S converted phases which were identified through receiver function analysis. They found that the MTZ was 10-30 km thicker than the global average in the areas surrounding the Mediterranean Sea (including the north-eastern parts of Libya). These findings were interpreted as resulting from past subduction. Bonatto et al. [2015] investigated the MTZ thickness beneath the Ibero-Magherbian region (to the west of the study area) using data from 258 seismic stations. Their method was also based on receiver function analysis and two different cross-correlation functions. They observed lateral variations in terms of the depths of the 410 km depth discontinuity (d410) and the 660 km depth discontinuity (d660) and the thickness of the MTZ which they attributed as the Betic-Aboran slab subducted beneath the Alboran Sea, as well as the presence of a garnet enriched layer beneath the western Moroccan region, and plume material beneath the Gulf of Cadiz.

The origin of Libya's volcanism (Tibesti, Al Haruj, As Saawada and Gharyan) and adjacent areas (Figure 1) is widely debated and many interpretations are based on mainly geochemical and isotopic data and rarely from regional geophysical studies [Elshaafi and Gudmundsson, 2018]. Previous models have mostly centered on two hypotheses. Some studies [e.g., Burke, 1996; Gourgaud and Vincent, 2004; Nixon et al., 2011] consider there to be a hotspot mantle plume beneath the region. By contrast, other studies [e.g., Lie´geois et al. 2005; Less et al., 2006] completely rule out the mantle plume theory.

Ebinger et al. [1989] propose that nearly all of the volcanic activity in North and Central Africa, such as the volcanoes found in Darfur, Tibesti and Cameroon, are associated with the Afar plume (Figure 1). The hypothesis relies on the lateral flow of plume materials beneath the lithosphere feeding the volcanoes in this region [Azzouni-Sekkal et al., 2007]. Keppie et al. [2011] offer a conceptual model based on geological constraints and geophysical data to depict the geometry of the super-plume underlying North Africa. This super-plume laterally feeds geographically discrete volcanic fields analogous to the Afar plume [cf. Ebinger aet a., 1989, 1998; Begg et al., 2009]. Burk [1996] proposes that the North African intraplate volcanism is related to mantle plumes in the underlying asthenosphere. Gourgaud and Vincent [2004] also allude to the existence of a mantle plume beneath the Tibesti volcanic province, southernmost Libya, using geochemical data.

By contrast, the tomographic model of Lie´geois et al. [2005] does not support the existence of mantle plumes beneath the Libyan volcanic provinces. This model instead assumes that the shallow mantle is warmer with melt fractions at depths between 100 km to 150 km. These estimated depths are in good agreement with the depths of 80-150 km reported from geochemistry and isotopic studies on the lavas and mantle xenoliths from the Al Haruj and Waw an Namous provinces [Bardintzeff et al., 2012]. In addition, the relatively low magmatic temperatures that have been obtained through the studied peridotite xenoliths (spinel lherzolites) [Peregi et al., 2003; Less et al., 2006; Elshaafi and Gudmundsson, 2017] from the Al Haruj Volcanic Province, do not support the presence of a mantle plume beneath this volcanic region but instead they suggest the existence of a relatively cold lithosphere. Beccaluva et al. [2007] suggest that the volcanism in Libya and adjacent regions is mostly related to passive asthenospheric mantle upwelling triggered by extensional stress in the lithosphere during Cenozoic reactivation. Cvetkovi´c et al. [2010]

proposed that volcanic activity was most likely initiated during the early stage evolution of the Sirt Basin.

Nixon et al. [2011] inferred that Libya's volcanism formed by diapirs and upwelling originating in the upper mantle. They concluded that the primary magmas originated at depths of 70 km for tholeiitic magmas with partial melt of 13.5% and 74 km for alkali magmas with partial melt of 18.9 %. The primitive mantle normalized multi-element patterns of Libya's basaltic rocks are highly enriched in incompatible trace elements, similar to within plate basalts, particularly oceanic island basalts (OIB) spectrum (St Helena-type) which represent basaltic melts from an enriched asthenospheric mantle source, most likely associated with an uprising mantle plume [Asran and Aboazom, 2004]. St. Helena is also formed by a mantle plume similar to that of many volcanic islands, such as Hawaii and Iceland.

Previous seismological investigations of the crust and mantle beneath Libya and adjacent areas have been global scale low-resolution studies [e.g., Pasyanos and Nyblade, 2007; Fishwick, 2010]. Tomography studies indicate that the volcanic areas in Libya are associated with a low-velocity mantle structure limited to the top 150 km [Lie´geois et al., 2005] as previously mentioned. Large positive velocity anomalies in the upper 100 km of North Africa were interpreted as the cratonic roots of cratonic terranes called the Sahara Metacraton [Grand, 2002; Lemnifi et al., 2015]. The delamination of cratonic roots have been proposed to explain the observed negative velocity anomalies at the depths of 100-175 km [Abdelsalam et al., 2011]. The interior of North Africa has also been imaged, with limited resolution,to show high velocity anomalies at depths above the 660 km discontinuity which suggests that the area is dominated by an accumulation of subducted slabs [Piromallo and Morelli, 2003]. The central portion of Libya was characterized as having a thinner lithosphere, which is about 90 to 100 km thick, based on studies of surface wave tomography

[Fishwick, 2010]. It is likely that partially molten magma reservoirs are active beneath the AS Sawda Volcanic Province (Figure 1), as detected recently by slow V_s waves in comparison to the V_p waves [Lemnifi et al. 2017a].

Most of the existing global or continental scale tomography models of the study area [Marone et al., 2003; Li´egeois et al., 2005; Pasyanos and Nyblade, 2007; Montagner et al., 2007; Fishwick, 2010; Bardintzeff et al., 2012] show weak anomalies but with limited depth investigation. P-and S-wave velocity perturbations have been observed in previous studies [e.g., Grand, 2002; Simmons et al., 2012]. Shear wave splitting measurements obtained adjacent to North Africa [Miller et al., 2013; Lemnifi et al., 2014; 2015] are attributed to mantle flow and represent the horizontal movement of the African continent to the north with local deflection of the mantle flow [Lemnifi et al., 2015].

The mantle layer between the 410 km and 660 km discontinuities (here after referred to as d410 and d660, respectively) is denominated as the Mantle Transition Zone (MTZ). Mineral physics and seismic studies [Ringwood, 1975] suggest that d410 is characterized as the phase transition from olivine to wadsleyite, while d660 is formed by the transformation of spinel to perovskite and magnesiowüstite. Previous determinations revealed Clapeyron slopes of +1.5 to +3.0 MPa K^{-1} for the olivine-wadsleyite (d410) 66 and -4.0 to -0.4 MPa K^{-1} for the post-spinel transition (d660) [Gao and Liu, 2014b; Tauzin and Ricard, 2014]. Therefore, the depths of the d410 and d660 phase changes are anticorrelated in depth of thermal anomalies. The d410 phase becomes shallower when it hosts colder material, and deeper with hotter material. The d660 phase exhibits the opposite behavior. As a consequence, the MTZ is thinner in higher temperature regions, and thicker in colder regions (such as near subducted slabs) [Helffrich, 2000; Lawrence and Shearer, 2006; Bonatto et al, 2015]. Previous studies have established that the depth variability of the d410 and

d660 can indicate the existence of cold subducted slabs and high temperature anomalies [e.g., Anderson, 1967; Collier et al., 2001; Contenti et al., 2012; Li & Yuan, 2003; Shearer & Masters, 1992; Wicks & Richards, 1993; Yu et al., 2017]. Kennett and Engdahl [1991] and Kennett et al. [1995] established that in most global models, the average thickness of the MTZ is 250 km, known because mineral phase variations between ?? olivine and ?? olivine occur at 410 km [Ringwood, 1975] and the spinel to bridgmanite variation occurs at 660 km [Ito & Katsura, 1989; Yamazaki & Karato, 2001].

Nevertheless, MTZ thickness variations depend not only on the temperature of the material, but also on water concentration and chemical composition [Gu et al., 1998; Flanagan and Shearer, 1998a; Meier et al., 2009]. Litasov et al. [2005] demonstrated that the presence of water within olivine, wadsleyite and ringwoodite has the effect of increasing the magnitude of the clapeyron slope and thus amplifies variations in depth. The effect is to deflect the d410 upward and the d660 downward, making it harder to observe the temperature changes, because thickening of the MTZ will always occur when a sufficient amount of water is present [Yu et al., 2017].

The present work focuses on MTZ studies by using new data from eighteen broadband seismic stations, which are managed by the Libyan Center for Remote Sensing, and Space Science (LCRSSS), in addition, data from three seismic stations are publically available and archived from the Incorporated Research Institutions for Seismology Data Management Center (DMC) (Figure 2). The main aim of this paper is using receiver function analysis to map the depth of the discontinuities and the thickness of the MTZ beneath Libya and so infer related geodynamical processes and understand better the origin of Libya's volcanism.

2. Data and Methods

Seismic data was requested from the Libyan Center for Remote Sensing and Space Science (LCRSS) with a recording time from early 2005 through late 2009. The dataset was enriched by the addition of 18 public broadband seismic stations, which operated between early 1990 to late 2016. The stations were located in the region between latitude 25° N and 36° N and longitude 4° E and 25° E (Figure 2), and the data was requested from the Incorporated Research Institutions for Seismology (IRIS) Data Management Center (DMC).

2.1 Receiver function stacking

The seismic events were selected based on epicentral distance, from 30° to 100° and cut-off magnitude, which is determined by the epicentral distance and focal depth, as defined by Liu and Gao [2010]. We calculated the receiver functions (RFs) based on the frequency-domain water-level deconvolution procedure [Ammon, 1991]. The seismograms were filtered in the frequency range of 0.02-0.50 Hz. An SNR-based procedure was applied to select high-quality RFs, further details about the quality of RFs are given by Gao and Liu [2014a]. Figure 3 shows global earthquakes and the number of RFs used in this study. We stacked the moveout-corrected RFs within each 2° radius bin based on the locations of the ray-piercing points at the depth of 535 km [Gao et al., 2014a]. We stack the RFs based on the piercing point locations calculated at each of the candidate discontinuity depths (e.g., Liu et al., 2003). The IASP91 reference Earth model [Kennett and Engdahl, 1991] was employed to stack the receiver functions using the non-plane wavefront assumption [Gao and Liu, 2014a]. RFs placed within each of the bins are resampled over 50 iterations [Efron & Tibshirani 1986; Liu et al. 2003; Dahm et al., 2017] to calculate the mean and standard deviation of the discontinuity depths and the thickness of the MTZ. The moveout-corrected RFs were converted into a depth range of 300–800 km with a vertical interval of 1 km.

Bins with less than 5 RFs were not used in this study in order to minimize the possibility of misidentifying the arrivals from the targeted discontinuities. In order to increase the reliability of the results, we manually picked the maximum amplitude near the theoretical arrival of the converted S waves from the MTZ discontinuities.

2.2 Travel-time residuals

To provide restrictions on the explanation on the observation of the results MTZ, we pick P-wave travel-time manually relative to the IASP91 Earth model on the vertical and transverse components, respectively. The P- and S-wave arrivals were measured relative to the IASP91 Earth model. The picking residuals accuracy is dependent on the signal strength relative to the background noise, as well as the sharpness of the arrivals (further details are given by Yu et al., 2015). In this study, we use 5.3 km s^{-1} for the P-waves.

We apply Equation (1) to correct for travel-times due to variations in station elevation [Nolet 2008; Yu et al., 2015].

$$\delta t_{ij}^{c} = \delta t_{ij} - \frac{hi}{v \; x \; cos[a \; sin \; (Rijx \; v)} \qquad (1)$$

where, δt_{ij} is the original residual (in seconds) found at the i^{th} station from the j^{th} event, R_{ij} is the ray parameter (in s km^{-1}), hi is the elevation (in km) for the i^{th} station, and v is the average velocity (in km s^{-1}) in the layer above sea-level.

3. Results

3.1 Apparent discontinuity depths and MTZ thickness

The RFs in the study area produced 162 bins with observable arrivals from the d410 and d660 (see Table S1 in the supporting information for all measurements). As shown in Figure 4, the P-to-S

conversion from the d410 and d660 can be easily identified when the traces are sorted according to depth. All of the stacked traces plot along eight latitudes from 27° N to 34° N as shown in Figure 5.

The average depth of the d410 in the study area is 413±6 km, and the average depth of the d660 is 663±8 km. The average MTZ thickness calculated is 249±14 km, which fully agrees with the IASP91 Earth model depth value of 250 km.

The observed depth of the d410 increases towards the central part of the study area, from approximately 400 km to 420 km (Figure 5a, b, c, e, and f). The apparent depth of the d660 increases from 650 to 670 km from longitudes 6° to 13°, but returns to 650 km from longitudes 14° to 28°. The depths of the d410 and the d660 increase by 10 km to 420 km and 670 km beneath the areas hosting volcanoes.

We find that the depths of the d410 and d660 are generally uncorrelated, and the cross-correlation coefficient (R) is 0.21 (Figure 6). To provide spatial series images for the results at the bins selected we used a continuous curvature surface gridding algorithm, with a tension factor of 0.5 (Smith &Wessel 1990; Yu et al., 2015). The Standard deviation (STD) of MTZ thickness in the region is less than 10 km (Figure 7d).

The weak correlation between the two depths studied indicates that the MTZ beneath the study area is influenced by materials with anomalously high or low temperatures [e.g., Bonatto et al, 2015]. MTZ thicknesses in the west and southeast are similar to the global average but the MTZ thickness in the northeast of Libya is about 20 km thicker than average (Figures 7c), while the south-central area, approximately centered at 14° E, 28° N, is about 10 km thinner. The thinnest portion of the MTZ, to the south of the As Sawda Volcanic Province (SVP), is affected by a

depressed d410 and an uplifted d660. Therefore, the weak correlation might indicate slower upper mantle velocities. To the northeastern part of Libya, a thicker MTZ is caused by shallowing of the d410 and deepening of the d660, which demonstrates a negative correlation between the d410 and d660 and as such indicates the presence of cold material. This finding is entirely supported by mineral physics studies [Ito and Takahashi, 1989; Fei, et al., 2004].

3.2 P-wave travel-time residual

We have hand-picked P-wave residuals from the teleseismic events (Figure 8). The observations represent the residuals from individual station-event pairs which are plotted at the ray-piercing point at the depth of 100 km from west to east along the study area. The P-wave traveltime residuals decrease in the central part of the region, and this again occurs spatially with the location of volcanic provinces.

4. Discussion

4.1. Spatial Variation of Anomalous MTZ Thicknesses and Temperatures

Here, our discussion will mainly focus in the area where the number of the RFs per station is high (above 105, see Figure 2). In Figure 3 to 7 and the following section we highlight several key features of the MTZ from the receiver function analysis. The MTZ is of constant thickness in the west of the studied region, thins by 10 km in the central part, and thickens by about 20 km beneath the northeastern part of Libya (Figure 7c). We infer that the location of the thinner MTZ (Figure 7c) is spatially related to the location of Quaternary volcanism, suggesting that there is a deep source of upwelling materials. To infer temperature changes the d410 Clapeyron slope of 2.9 MPa/K [Bina and Helffrich, 1994], and the d660 Clapeyron slope of -2.1 MPa/K [Fei et al., 2004] are adopted. Therefore, considering that our results show a standard variation of the MTZ thickness

of 14 km, this is equivalent to normal thermal variations of ±76° K. The change in MTZ thickness to 20 km thinner-than-average as controlled by deepening d410 corresponds to an excess temperature of 242° K centered in the central and northwestern part of Libya, implying higher temperatures in the transition zone beneath central Libya.

Mohamed et al. [2014] adapted several different models that take account of velocity, thermal, and water content anomalies in order to explain the variations in thickness of the MTZ beneath the Afro-Arabian Dome. Those models relate the change in MTZ discontinuity depths to the effect of olivine- and garnet-dominated phase changes, and MTZ hydration. The variation in thickness of the MTZ in the area of investigation can be most appropriately fitted to two of the proposed models of Mohamed et al. [2014]. The first model explains that the thinnest part of the MTZ occurs because Libya's Quaternary volcanism is underlain by low seismic velocities in the upper and lower mantle. In the first model, the main depression occurs in the d410, with uplift in the d660, which corresponds to the observed values between the longitudes from 14° to 20° in the central part of this region. This agrees with the findings of Fishwich [2010] who found that the lithosphere is about 90 km thinner beneath this area. Given the fact that the area with the thinned MTZ has a thinner lithosphere, this model indicates that the upwelling material probably originated from the lower mantle. This is in agreement with a proposed heat source originating in the lower mantle that drives Cenozoic volcanism in northwest Africa (e.g., Hoggar) [Courtillot et al., 2003]. Courtillot et al. (2003) suggest that hotspots may derive from distinct mantle boundary layers. Thus, our findings propose that the origin of Libya's volcanism may come from higher-than-normal temperatures in the mantle transition zone (MTZ).

4.2 MTZ hydration

Apparently depressed MTZ discontinuities can also be explained through hydration mechanisms [Reed et al., 2016]. The presence of water assists both to thicken the MTZ through an immediate uplift and depression of the d410 and d660 (Figure 7), respectively, and to decrease the seismic velocities in the MTZ. The occurrence of a strong, continuous 520 km discontinuity and also a negative arrival immediately above the d410 beneath Afar is expressive of hydrous upwelling across the MTZ [Thompson et al., 1992; 2015; Reed et al., 2016]. In principle, the thickening of the MTZ observed in the eastern part of the region can also be caused by the presence of water. Though, some studies proposed that under normal pressure temperature conditions [Yu et al., 2017], water might promote a low-velocity anomaly of the phase transition associated with the d410. This process would cause anomalously low stacking amplitudes [Wood, 1995].

The velocity anomalies of about 0.5 s observed from picking P-wave travel-time velocities, fit well with what we observe at the volcanic provinces in the study area, especially at the As Sawda volcanic province (Figure 8). The profile from east to west of the study area observed through P-wave travel-time velocities shows a low average velocity in the central part of Libya where most of the volcanic provinces occur.

4.3 Slab Segments in the MTZ

Water has previously been used to explain low-velocity anomalies associated with phase transitions at the d410 [Tauzin et al., 2010]. Thicker portions of the MTZ in the northeastern part of Libya are caused partly by hydrated minerals, resulting in a general increase in water content. This hydration could be associated with African-Eurasian closure and the subduction of the Tethys Ocean plate [Stern, 1994]. The thickening of the MTZ observed in other areas can also be caused by the presence of water [e.g., Litasov et al., 2005; Yu et al., 2017].

A positive anomaly at the depths of 400 to 600 km beneath the northeastern part of Libya likely reflect part of the past subduction of the Thethys slab [Simmons et al., 2012] (Figure 7). Here, we suggest that the thicker MTZ is related to 170°K colder-than-normal temperatures, since cooler temperatures are related to positive velocity anomalies. Higher water contents also cause anomalously low stacking amplitudes or the presence of negative receiver function signals at the upper portion of the d410 discontinuity [Bercovici and Karato, 2003]. The velocity anomalies found in this study match this observation. Generally, tomographic studies using the global S-wave model by Grand [2002] and P-wave model by Piromallo and Morelli [2003] indicate the positive velocity anomaly observed in the eastern part of the study area. Also, our analysis of the P-wave travel-time residuals indicate a slightly higher average velocity (Figure 8). Given the fact that the northeastern part of Libya has a thickened MTZ, this is likely a reflection of past subduction and African-Eurasian collision since the late Mesozoic, and is also in agreement with the findings and interpretation of Van der Meijde at al. [2005] and Bonatto et al. [2015] in neighboring areas.

4.4 Preliminary Model

The existence of an active mantle plume beneath northern-central Africa has been proposed based on geophysical studies [e.g., Lie´geois et al. 2005], geological constraints, geophysical data [Keppie et al. 2011], and geochemical studies [Gourgaud and Vincent, 2004]. The total MTZ depression in the study area is estimated to be 10 km beneath the volcanic provinces (using a Clapeyron slope of 2.9 MPa/K; Figure 5d, and e). Similarly, there is a reported uplift of the d660 using a Clapeyron slope of -2.1 MPa/K [Fei et al., 2004]. Therefore, the plume model would produce a net 20 km thinning of the MTZ (Figure 7). This is quite different to the eastern part of Libya where there is uplifted d410 and depressed d660 which has led to a thickening of the MTZ.

As such, the existence of partial melts in the upper mantle [Lemnifi et al., 2017a] and the MTZ can also affect the range of MTZ thicknesses.

As demonstrated by previous studies [e.g., Liĕgeois et al., 2005] the source of partial melt is derived from the uppermost mantle (less than 150 km) during the reactivation of shear zones during the African-Eurasian collision. Contrarily, Nixon et al. [2011] inferred from geochemical data that the primary magmas in central Libya were instead derived from depths of between 70 km to 74 km at temperatures of around 1360°C. In this area, the maximum depression of the d410 is at 28° N. At the same location, the apparent depression of the d660 is about 10 km, leading to a 20 km apparent thinning of the MTZ suggesting that the partial melting and magma reservoirs occur much deeper. We therefore encourage the installation of more broadband seismic stations around the volcanic provinces in order to provide higher resolutions and spatial coverages and so in order to address these apparently contradictory models.

A thicker-than-normal MTZ is revealed to the eastern part of the area at latitudes from 28° N to 32° N and longitudes 6°E to 13°E as shown in Figure 7c. These thicker-than-normal MTZ features are found adjacent to slab segments which were also inferred from the thick MTZ and high MTZ velocities (Figure 5 d, e, and f). Within the central part of the area, the MTZ is thinner-than-normal. This area is also host to pervasive Cenozoic volcanism and is characterized by an apparent depression of the d410 of about 10–15 km. Our preferred model for this study is illustrated in Figure 9, where a warm thermal anomaly causes a depression of the d410 in the central part of Libya. We hope that these results encourage further research into the origin of Libya's volcanism.

4.5 Consequences for the deposition of minerals

It is well recognized that the geometrical arrangement of crustal structures influences the deposition of hydrothermal minerals [Hildenbrand et al., 2000]. Whilst the relationship between ore formation and lithospheric thickness is still poorly constrained and unknown some inferences about potential mineralization in the Libyan region can be hypothesized.

We broadly categorize the region into an area hosting a thinner-than-normal mantle transition zone (and so thicker lithosphere) and an area hosting a thicker-than-normal mantle transition zone (and so a thinner lithosphere) (Figure 9). The thinner MTZ is characterized by increased melt production which is associated with numerous shear and extensional fractures such as ring-faults and dykes as well as presumably significant hydrothermal circulation. The location of epithermal and porphyry precious and base metal deposits may then form in such environments, whereas they are less likely to form in the colder stagnant slab region (Figure 9). Further studies are certainly still needed in the future in order to obtain better constraints on the ore deposits in Libya.

5. Conclusions

This is the first study to investigate the d410 and d660 depth variations, and mantle transition zone thicknesses beneath Libya using receiver functions. This marks an important step in the quest to understand tectonic processes in the northern portion of the African continent. The results show that the d410 was depressed, while the d660 was uplifted within the Miocene – Quaternary volcanic areas and an anomalously thin MTZ in the central portion of Libya suggests that the Miocene – Holocene volcanoes heat source originated within the lower mantle. Hence, our findings propose that the origin of Libya's volcanism may derive from higher temperatures in the mantle transition zone (MTZ), deeper than 410 km, beneath this region. This conclusion is in good agreement with the hypothesis of a mantle plume where Miocene-Holocene volcanic activity

throughout Libya was/is directly related to an uprising mantle plume rather than related solely to extension of the lithosphere. Conversely, the MTZ is thickened in the north-east to approximately 270 km, indicating a colder-than-average MTZ. We infer that this thicker and colder MTZ is most likely associated with slab stagnation.

Acknowledgments.

We thank the participants of the Libyan Center for Remote Sensing and Space Science (LCRSSS) and the IRIS DMC for providing the high-quality seismic data used in the study. We are grateful to Kelly Liu, Stephen Gao and Bruno Goetza for helpful discussions and comments. The study was supported by the Benghazi University, Libya.

References

Abdelsalam, M.G., Gao, S.S., Ligeois, J.P., 2011. Upper mantle structure of the Saharan Metacraton. J. Afr. Earth Sci., 60, 328-336, doi:10.1016/j.jafrearsci.2011.03.009.

Anderson, D. L., 1967. Phase changes in the upper mantle. Science, 157, 1165–1173.

Ammon, C.J., 1991. The isolation of receiver effects from teleseismic P250 waveforms. Bull. Seismo. Soc. Amer., 81, 2,504-2, 510.1.

Asran AMH, Aboazom AS (2004) CRZ Al-Haruj tertiary basalts, Libya: petrological and geochemical approach. In: Proceedings of the 6th international conference on the geology

of the Arab World (GAW6).

Azzouni-Sekkal, A., Bonin, B., Benhallou, A., Yahiaoui, R., Liégeois, J., 2007. Cenozoic alkaline volcanism of the Atakor massif, Hoggar, Algeria, J. Soci. Amer., 418, p. 321–340, doi: https://doi.org/10.1130/2007.2418(16)

Bardintzeff, J.M., Deniel, C., Guillou, H., Platevoet, B., T´elouk, P., Oun, K.M., 2012. Miocene to recent alkaline volcanism between Al Haruj and Waw an Namous (southern Libya). J. Inter. Earth Sci., 101(4), 1047-1063, doi:10.1007/s00531-011-0708-5.

Beccaluva, L., Azzouni-Sekkal, A., Benhallou, A., Bianchini, G., Ellam, R.M., Marzola, M., Siena, F., Stuart, F.M., 2007. Intracratonic asthenosphere upwelling and lithosphere rejuvenation beneath the Hoggar swell (Algeria): evidence from HIMU metasomatised lherzolite mantle xenoliths. Earth Planet. Sci. Lett., 260(3), 482-494, doi:10.1016/j.epsl.2007.05.047.

Begg, G. C., et al., 2009. The lithospheric architecture of Africa: Seismic tomography, mantle petrology, and tectonic evolution, Geosphere, 5, 23–50, doi:10.1130/GES00179.

Bina C.R., Helffrich, G., 1994. Phase-transition Clapeyron slopes and transition zone seismic discontinuity topography. J. Geophys. Res., 99(B8):15853-15860.

Bonatto, L., Schimmel, M., Gallart, J., Morales, J., 2015. The upper-mantle transition zone beneath the Ibero-Maghrebian region as seen by teleseismic Pds phases. Tectonophysics, doi.org/10.1016/j.tecto.2015.02.002.

Burke, K., 1996, The African plate: South African Journal of Geology, v. 99, p. 339–410.

Capitanio, F.A., Faccenna, C., Funiciello, R., 2009. The opening of Sirte basin: Result of slab avalanching? Earth Planet. Sci. Lett., 285(1), 210-216, doi:10.1016/j.epsl.2009.06.019.

Collier, J. D., Helffrich, G. R., Wood, B. J., 2001. Seismic discontinuities and subduction zones. Physics of the Earth and Planetary Interiors, 127, 35–49.

Contenti, S., Gu, Y. J., Okeler, A., Sacchi, M. D., 2012. Shear wave reflectivity imaging of the Nazca-South America subduction zone: Stagnant slab in the mantle transition zone? Geophysical Research Letters, 39, L02310. https://doi.org/10.1029/2011GL050064

Courtillot, V., Davaille, A., Besse, J., Stock, J., 2003. Three distinct types of hotspots in the Earth‘s mantle. Earth Planet. Sci. Lett., 273 v. 205, p. 295-308, doi: 10.1016/S0012-821X (02)01048-8.

Cvetkovi´c, V., Tolji´c, M., Ammar, N.A., Rundi´c, L., Trish, K.B., 2010. Petrogenesis of the eastern part of the Al Haruj basalts (Libya). J. African Earth Scie., 58(1), 37-50, doi: 10.1016/j.jafrearsci.2010.01.006.

Dahm, H. H., Gao, S. S., Kong, F., Liu, K. H., 2017. Topography of the mantle transition zone discontinuities beneath Alaska and its geodynamic implications: Constraints from receiver function stacking. J. Geophys. Res. Solid Earth. 122, 10,352–10,363. https://doi.org/10.1002/2017JB014604

Ebinger, C. J., Deino, A. L., Drake, R. E., Tesha A. L., 1989. Chronology of volcanism and rift basin propagation: Rungwe volcanic province, East Africa, J. Geophys. Res., 94, 15,785–15,803.

Efron, B., Tibshirani, R., 1986. Bootstrap methods for standard errors, confidence intervals, and other measures of statistical accuracy. Statistical Science, 1, 54–75.

Elshaafi, A., Gudmundsson A., 2018. Mechanical interaction between volcanic systems in Libya. Tectonophysics, 722, 549-565, doi.org/10.1016/j.tecto.2016 .11.031.

Elshaafi, A., Gudmundsson, A., 2017. Distribution and size of lava shields on the Al Haruj al Aswad and the Al Haruj al Abyad Volcanic Systems, Central Libya. J Volcanol Geotherm

Res 338:1–17.Faccenna, C., et al., 2014. Mantle dynamics in the Mediterranean. Rev. Geophys., 52, 283-332, doi:10.1002/2013RG000444.

Elshaafi, A., Gudmundsson, A., 2016. Volcano-tectonics of the Al Haruj Volcanic Province, Central Libya. J. Volcanol. Geotherm. Res. 325:189–202.

Fei, Y., et al., 2004. Experimentally determined postspinel transformationboundary in Mg2SiO4 using MgO as an internal pressure standard and its geophysical implications. J. Geophys. Res.: Solid Earth (1978-2012), 109(B2), doi:10.1029/2003JB002562.

Fishwick, S., 2010. Surface wave tomography: Imaging of the lithosphere asthenosphere boundary beneath central and southern Africa?, Lithos., 120.1: 63-73.

Flanagan, M.P., Shearer, P.M., 1998a. Global mapping of topography on transition zone velocity discontinuities by stacking SS precursors. J.Geophys. Res. 103 (B2), 2673-2692.

Gao, S.S., Liu, K.H., 2014a. Imaging mantle discontinuities using multiply-reflected P-to-S conversions. Earth Planet. Sci. 294 Lett., 402, 99-106, doi.org/10.1016/j.epsl.2013.08.025.

Gao, S. S., Liu, K.H., 2014b. Mantle transition zone discontinuities beneath the contiguous United States. J. Geophys. Res., 119, 6,452-6,468, doi.org/10.1002/2014JB011253.

Grand, S.P., 2002. Mantle shear-wave tomography and the fate of subducted slabs. Philos, Trans. R. Soc. London A, 360, 2475-2491, doi:10.1098/rsta.2002.1077.

Gu, Y., Dziewonski, A.M., Agee, C.B., 1998. Global de-correlation of the topography of transition zone discontinuities. Earth Planet. Sci. Lett. 157, 57-67.

Gourgaud A, Vincent P. M., 2004. Petrology of two continental alkaline intraplate series at Emi Koussi volcano, Tibesti, Chad. J. Volcanol. Geotherm. Res., 129:261–290

Hassan, H.S., Kendall, C.G., 2014. Hydrocarbon provinces in Libya: A petroleum system study,

in Petroleum Systems of the Tethyan Region, AAPG Mem., vol. 106, edited by R. Marlow, C. Kendall, and L. Yose, pp.1-43, American Association of Petroleum Geologists, Tulsa, Oklahoma.

Helffrich, G., 2000. Topography of the transition zone seismic discontinuity,Rev. Geophys. 38, \ 141-158.

Hildenbrand, T. G., Berger, B., Jachens, R. C., & Ludington, S. 2000. Regional crustal structures and their relationship to the distribution of ore deposits in the western United States, based on magnetic and gravity data. *Economic Geology*, *95*(8), 1583-1603.

Hoernle, K., Zhang, Y.S., Graham, D., 1995. Seismic and geochemical evidence for large- scale mantle upwelling beneath the eastern Atlantic and western and central Europe. Nature, v. 374, p. 34-39, doi:10.1038/374034a0.

Ito, E., Takahashi, E., 1989. Postspinel transformations in the system Mg2SiO4-Fe2SiO4 and some geophysical implications. 316 J. Geophys Res. 94:10 637-10 646.

Kennett, B.L.N., Engdahl, E.R., 1991. Traveltimes for global earthquake location and phase identification. J. Geophys. Intern., 105(2), 429-465, doi: 10.1111/j.1365-246X.1991.tb06724.x.

Kennett, B. L. N., Engdahl, E. R., Buland, R., 1995. Constraints on seismic velocities in the Earth from traveltimes. Geophysical Journal International, 122, 108–124.

Lawrence, J.F., Shearer, P.M., 2006. A global study of transition zone thickness using receiver functions. J. geophys. Res., 111, B06307, doi:10.1029/2005JB003973.

Lemnifi, A.A., Liu, K. H., Gao, S. S., Elsheikh, A. A., Reed, C. A., Yu, Y., and Elmelade, A. A., 2014. Investigations of Libya Upper Mantle Anisotropy and Crustal Structure Using Shear wave Splitting and Receiver Function Analyses, Eos Trans. AGU, Fall Meet.

Lemnifi, A.A., Liu, K.H., Gao, S.S., Reed, C.A., Elsheikh, A.A., Yu, Y., Elmelade, A.A., 2015.

Azimuthal anisotropy beneath north central Africa from shear wave splitting analyses. Geochem. Geophys. Geosyst., 16, doi:10.1002/2014GC005706.

Lemnifi, A., Elshaafi, A., Browning, J., El Ebadi, S., Gudmundsson, A., 2017a. Crustal thickness beneath Libya and the origin of partial melt beneath AS Sawda Volcanic Province from receiver-function constraints. J. Geophys. Res. Solid Earth. http://dx. doi.org/10.1002/2017JB014291.

Lemnifi, A. A., Elshaafi, A., Karao˘glu, Ö., Salah, M. K., Aouad, N., Reed, C. A., & Yu, Y., 2017b. Complex seismic anisotropy and mantle dynamic beneath Turkey. J. Geodynamics, 0264–3707. https://doi.org/10.1016/j.jog.2017.10.004.

Less, G., Turki, S., Suwesi, K., Peregi, L., Koloszar, L., Kalmar, J., Sherif, K., Csaszar, G., Gulasci, Z., Dalum, H., Al Tajuri, A., 2006. Explanatory Booklet. Geological Map of Libya 1: 250.000. Sheet: Waw Al Kabir NG 33-12. Industrial Research Centre, pp. 295.

Li, X., Yuan, X., 2003. Receiver functions in northeast China—Implications for slab penetration into the lower mantle in northwest Pacific subduction zone. Earth and Planetary Science Letters, 216, 679–691. https://doi.org/10.1016/S0012-821X(03)00555-7

Li´egeois, J.P., Benhallou, A., Azzouni-Sekkal, A., Yahiaoui, R., Bonin, B., 2005. The Hoggar swell and volcanism: reactivation of the Precambrian Tuareg shield during Alpine convergence and West African Cenozoic vocanism. Geolog. Soci. Amer. Special Papers, 388, 379-400, doi:10.1130/0-8137-2388-4.379GSA Special Papers 2005, v. 388, p. 379-400.

Litasov, K.D., Ohtani, E., Sano, A., Suzuki, A., Funakoshi, K., 2005. Wet subduction versus cold subduction. Geophys. 338 Res. Lett., 32, L13312, doi:10.1029/2005GL022921.

Liu, K. H., Gao, S. S., Silver, P. G., Zhang, Y. K., 2003. Mantle layering across central South America. Journal of Geophysical Research, 108(B11), 2510.

https://doi.org/10.1029/2002JB002208

Liu, K.H., Gao, S.S., 2010. Spatial variations of crustal characteristics beneath the Hoggar swell, Algeria, revealed by systematic analyses of receiver functions from a single seismic station. Geochem. Geophys. Geosyst., 11, Q08011, doi:10.1029/2010GC003091.

Marone, F., Van Der Meijde, M., Van Der Lee, S., Giardini, D., 2003. Joint inversion of local, regional and teleseismic data for crustal thickness in the Eurasia-Africa plate boundary region. J. Geophys. Intern., 154(2), 499-514, doi: 10.1046/j.1365-246X.2003.01973.x.

Meert, J.G., Lieberman, B.S., 2008. The Neoproterozoic assembly of Gondwana and its relationship to the Ediacaran-Cambrian radiation. Gondwana Res., 14, 5-21, doi:10.1016/j.gr.2007.06.007.

Meier, U., Trampert, J., Curtis, A. (2009). Global variations of temperature and water content in the mantle transition zone from higher mode surface waves. Earth Planet. Sci. Lett., 282, 91-101, doi:10.1016/j.epsl.2009.03.004.

Miller, M.S., Allam, A.A., Becker, T.W., Di Leo, J.F., Wookey, J., 2013. Constraints on the tectonic evolution of the westernmost Mediterranean and northwestern Africa from shear wave splitting analysis. Earth Planet. Sci. Lett., 375, 234-243, doi:10.1016/j.epsl.2013.05.036.

Mohamed, A.A., Gao, S.S., Elsheikh, A.A., Liu, K.H., Yu, Y., Fat-Helbary, R.E., 2014. Seismic imaging of mantle transition zone dis-continuities beneath the northern Red Sea and adjacent areas. 361 J. Geophys. Int., 199, 648-657, doi.org/10.1093/gji/ggu284.

Montagner, J.-P., et al., 2007. Mantle upwellings and convective instabilities revealed by seismic tomography and helium isotope geochemistry beneath eastern Africa. Geophys. Res. Lett., 34, L21303, doi:10.10129/2007GL031098.

Nixon, S., Maclennan, J., White, N., 2011. Intra-plate magmatism of the Al Haruj Volcanic Field, Libya. In: Goldschmidt Conference Abstracts.

Nolet, G., 2008. A Breviary of Seismic Tomography, Cambridge Univ. Press.

Pasyanos, M.E., Nyblade, A.A., 2007. A top to bottom lithospheric study of Africa and Arabia. Tectonophysics, 444(1), 27-44, doi:10.1016/j.tecto.2007.07.008.

Peregi, Z., Less, G., Konrad, G., Fodor, L., Gulacsi, Z., Gyalog, L., Turki, S., Suwesi, S., Sherif, Kh., Dalub, H., 2003. Explanatory Booklet. Geological Map of Libya 1: 250.000. Sheet: Al Haruj Al Abyad NG 33-8. Industrial Research Centre, Tripoli, pp. 248.

Piromallo, C., Morelli, A., 2003. P wave tomography of the mantle under the Alpine-Mediterranean area. J. Geophys. Res.: Solid Earth (1978-2012), 108(B2), doi:10.1029/2002JB001757.

Reed, C. A., Liu, K. H., Chindandali, P. R. N., Massingue, B., Mdala, Mutamina, H., D., Yu, Y., Gao, S. S., 2016. Passive rifting of thick lithosphere in the southern East African Rift: Evidence from mantle transition zone discontinuity topography. J. Geophys. Res., 121, 8068–8079, doi:10.1002/2016JB013131.

Ringwood, A. E., 1975. Composition and Petrology of the Earth‘s Mantle, 1st edn, pp. 672,

Shearer, P. M., & Masters, T. G., 1992. Global mapping of topography on the 660-km discontinuity. Nature, 355, 791–796.McGraw-Hill, New York.

Simmons, N.A., Myers, S.C., Johannesson, G., Matzel, E., 2012. LLNLG3Dv3: Global Pwave tomography model for improved regional and teleseismic travel time prediction. J. Geophys. Res.: Solid Earth (1978-2012), 117(B10), doi:10.1029/2012JB009525.

Stern, R.J., 1994. Arc-assembly and continental collision in the Neoproterozoic African orogen: Iimplications for the consolidation of Gondwanaland, Annu. Rev. Earth Planet. Sci., 22, 319-351, doi.org/10.1146/annurev.ea.22.050194.001535.

Tauzin, B., Debayle, E., Wittlinger, G., 2010. Seismic evidence for a global low velocity layer in

the Earth's upper mantle. Nat. Geosci. 3, 718. doi:10.1038/NGEO969.

Tauzin, B., Ricard, Y., 2014. Seismically deduced thermodynamics phase diagrams for the mantle transition zone. Earth Planet. Sci. Lett. 401, 337–346, https://doi.org/10.1016/j.epsl.2014.05.039.

Thompson, A.B., 1992. Water in the Earth's upper 383 mantle. Nature, 358, 295-302, doi:10.1038/358295a0.

Thompson, D. A., Hammond, J. O. S., Kendall, J.-M., Stuart, G. W., Helffric, G. R. h, Keir, D., Ayele, A., Goitom, B., 2015. Hydrous upwelling across the mantle transition zone beneath the Afar Triple Junction. Geochem. Geophys. Geosyst., 16, 834–846, doi:10.1002/2014GC005648.

Van der Meijde, M., Van der Lee, S., Giardini, D., 2005. Seismic discontinuities in the Mediterranean mantle. Physics the Earth Planet. Inter., 148(2), 233-250, doi:10.1016/j.pepi.2004.09.008.

Wang, X., Niu, F., 2011. Imaging the mantle transition zone beneath eastern and central China with CEArray receiver functions. Earthquake Sci., 24(1), 65-75.

Wang, B., Niu, F., 2010. A broad 660 km discontinuity beneath northeast China revealed by dense regional seismic networks in China. J. Geophys. Res.: Solid Earth (1978-2012), 115(B6), doi:10.1029/2009JB006608.

Wang, T., Chen, L., 2009. Distinct velocity variations around the base of the upper mantle beneath northeast Asia. Phys. Earth Planet. Interio., 172(3), 241-256, doi:10.1016/j.pepi.2008.09.021.

Wood, B. J., 1995. The effect of H2O on the 410-kilometer seismic discontinuity, Science, 268, 74–76.

Yamazaki, D., & Karato, S., 2001. Some mineral physics constraints on the rheology and

geothermal structure of Earth's lower mantle. American Mineralogist, 86, 385–391. https://doi.org/10.2138/am-2001-0401

Yu, Y., S. S. Gao, K. H. Liu, T. Yang, M. Xue, and K. Phon Le (2017), Mantle transition zone discontinuities beneath the Indochina Peninsula: Implications for slab subduction and mantle upwelling, Geophys. Res. Lett., 44, 7159–7167, doi:10.1002/2017GL073528.

Figure Caption

Figure 1. Topographic map showing the main geological features in the study area and neighboring areas. The dashed black lines show the locations of the main volcanic provinces in the Libyan territory. The main Mesozoic rifts with teeth on downthrown blocks are shown by black lines. The blue dashed line shows the location of the vertical cross-section in Figure 9. Inset map shows the location of the study area in Africa. The blue solid lines show the east African rift.

Figure 2. Topographic map overlaid with circles representing the central point of each 2◦ radius bins. The triangles represent the seismic stations used in this study. HA: Hellenic Arc. The different sizes of the triangles represent the number of RFs obtained from each station. The color of the circles represents the number of RFs per bin.

Figure 3. Spatial distribution of earthquakes. Each dot represents earthquake events within a 2° radius area. The color of the dots represents the number of earthquake events within each circle.

Figure 4. (a) The results of stacking normal moveout-corrected RFs, plotted with the sequentially increasing depth of the d410, and (b) same as (a) but for the d660.

Figure 5. Profiles showing the RFs stacked in 2° radius bins at depths from 350 km and 750 km along eight latitudes. Thick gray lines of the stacked RFs shows the depth series average; black lines around it represent the mean ± 2σ; black circles represent the average depths of the d410 and the d660, with error bars showing 2σ of the peaks depth.

Figure 6. Cross correlation plot (R) of the d410 and d660 apparent depths. The error bars represent the **(σ)** standard deviation.

Figure 7. (a) Results showing the topography of the d410, (b) same as (a) but for the d660, (c) MTZ thickness, and (d) MTZ standard deviation (STD). Contour lines are spaced at 10 km intervals for in (a)-(c), but at 2 km (d).

Figure 8. Teleseismic P-wave traveltime residuals displayed above the ray-piercing points at 100 km depth and projected from west to east of the study area. The red points are individual event values, and circles with error bars are station-averaged values.

Figure 9. Schematic explanation for the proposed model, where the topography of the 410 and 660 discontinuities change along section from SW to NE in the study area.

Figr-1

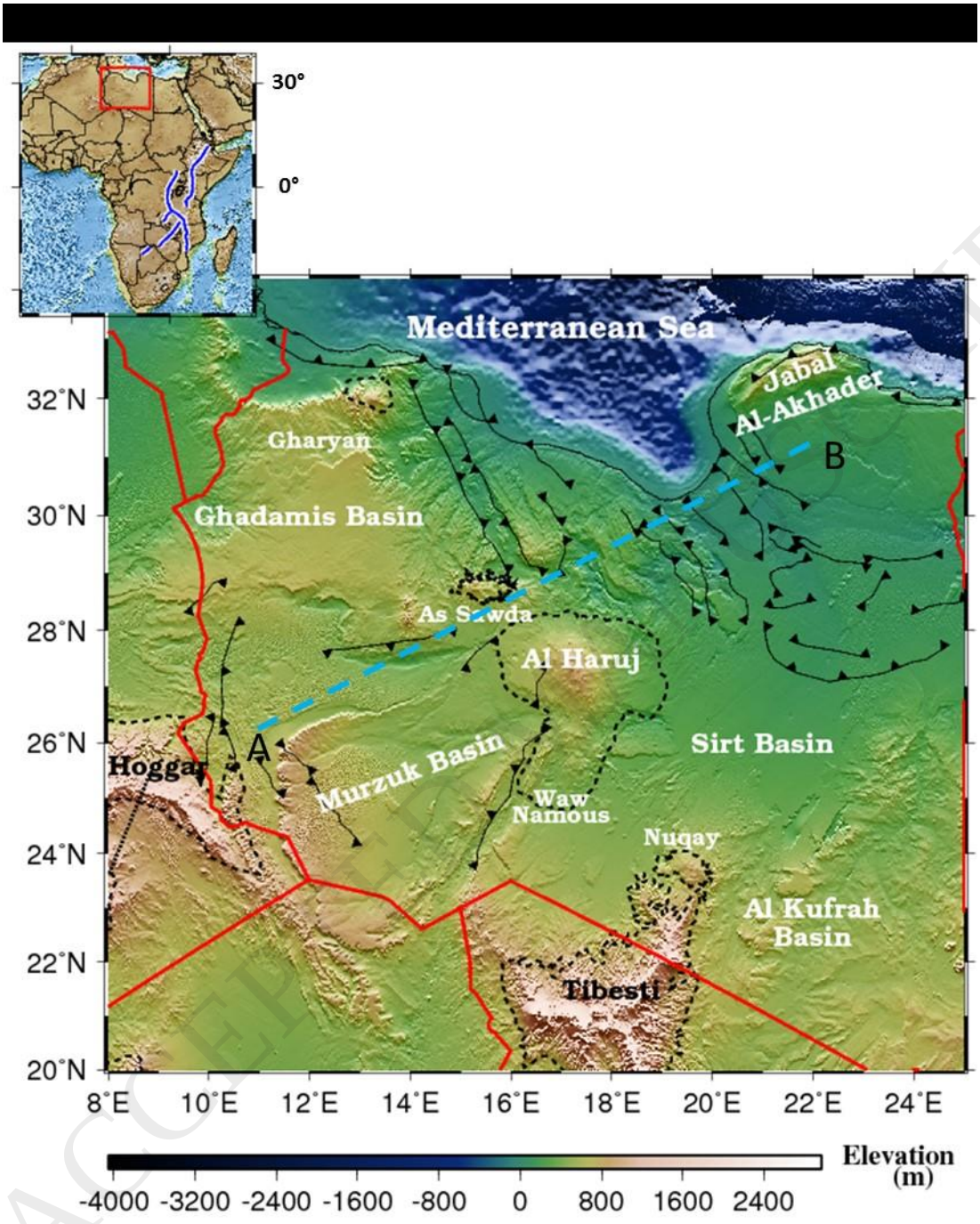

Figr-2

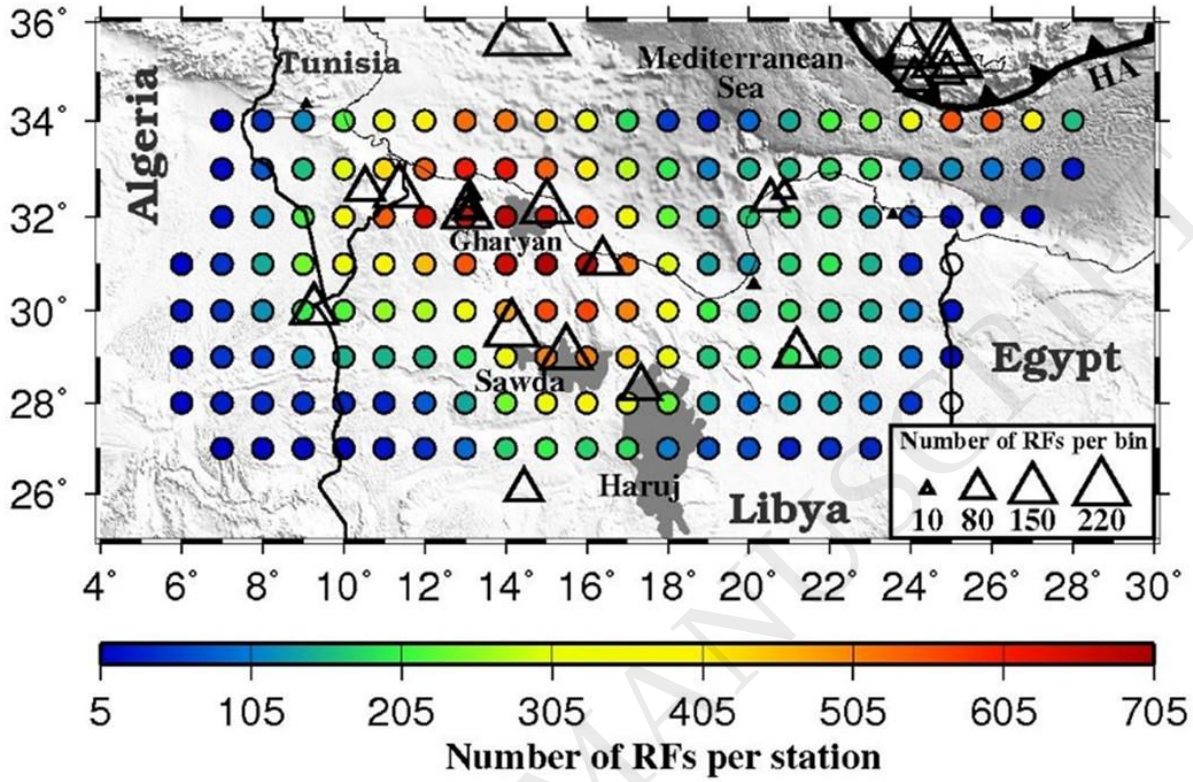

Figr-3

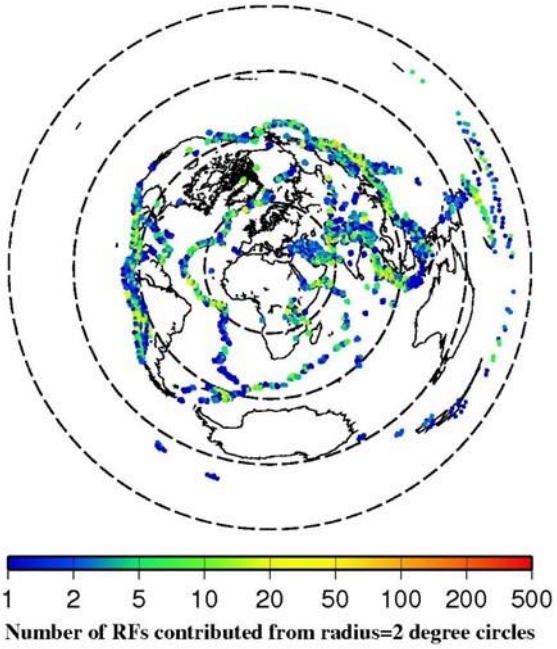

Figr-4

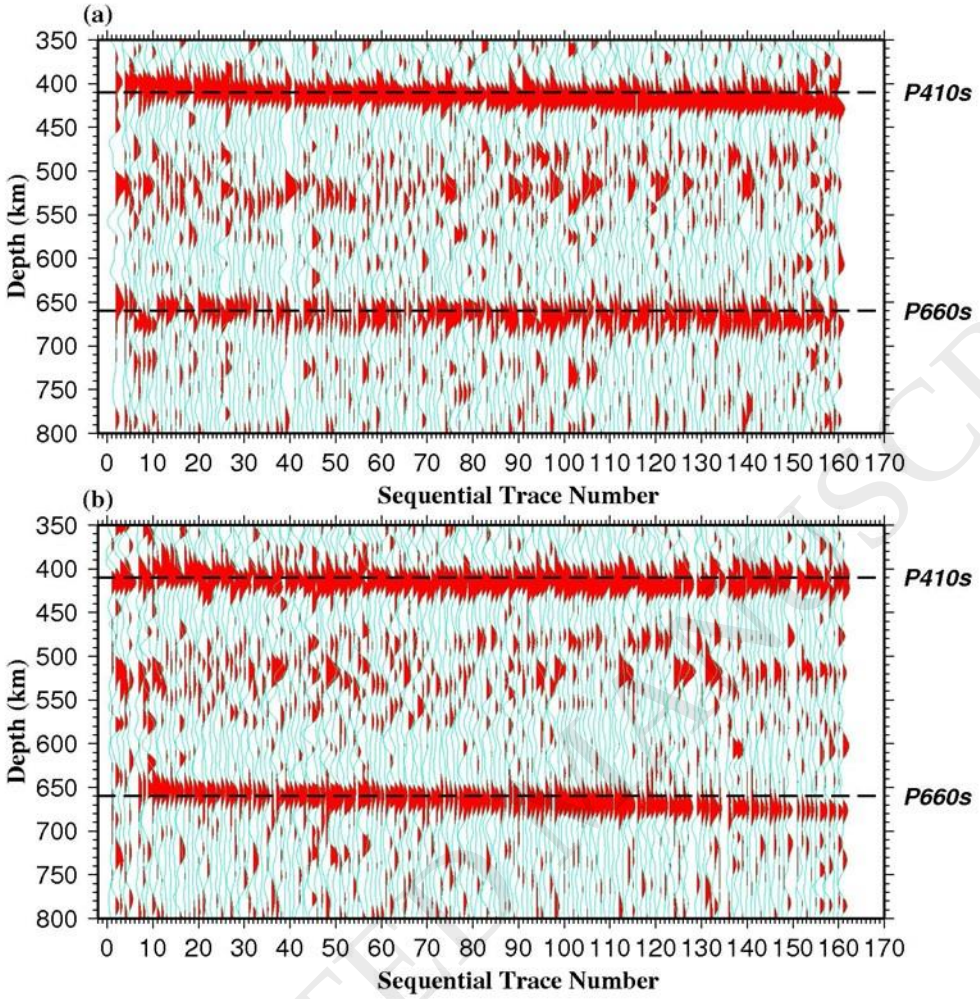

Figr-5

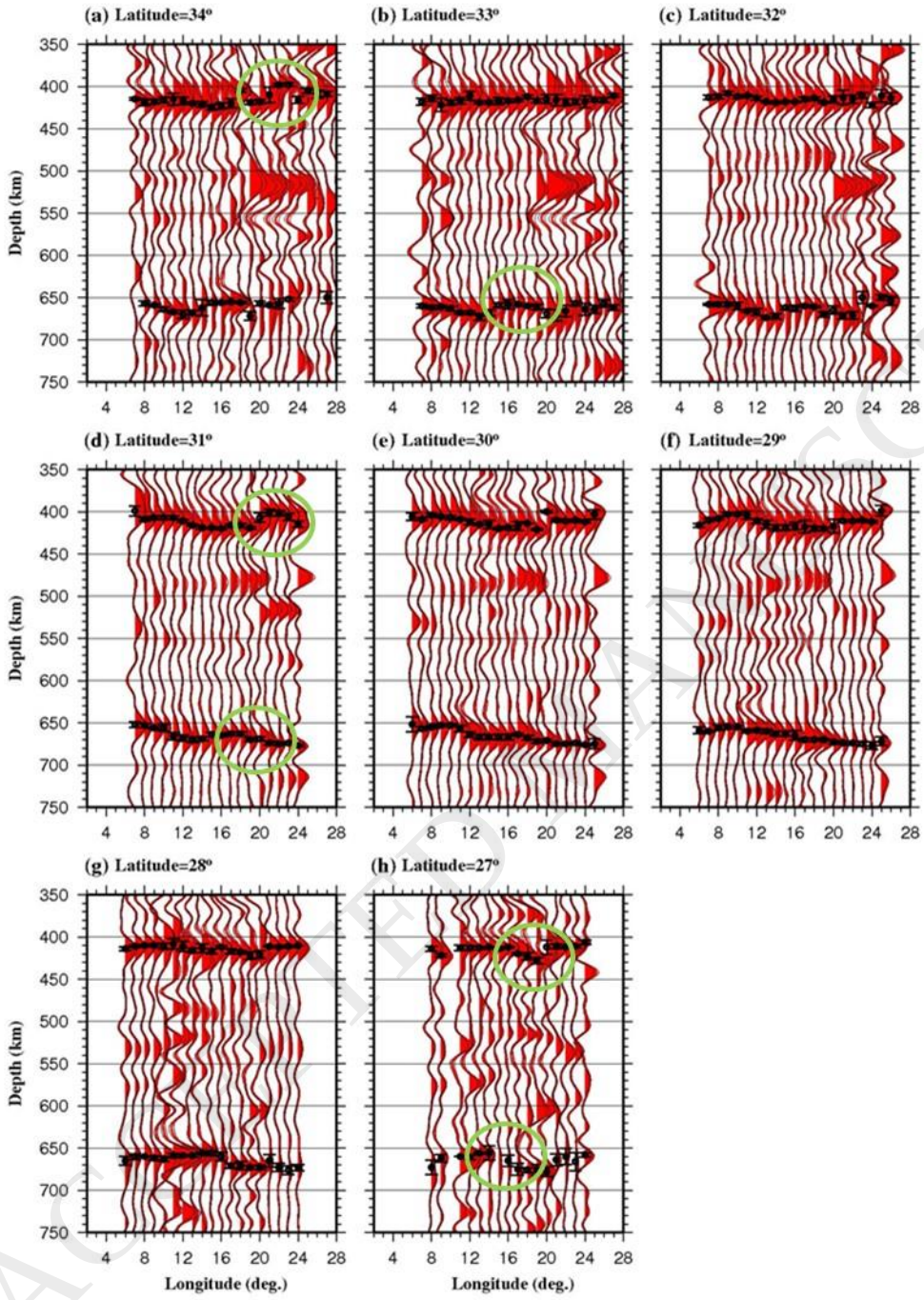

Figr-6

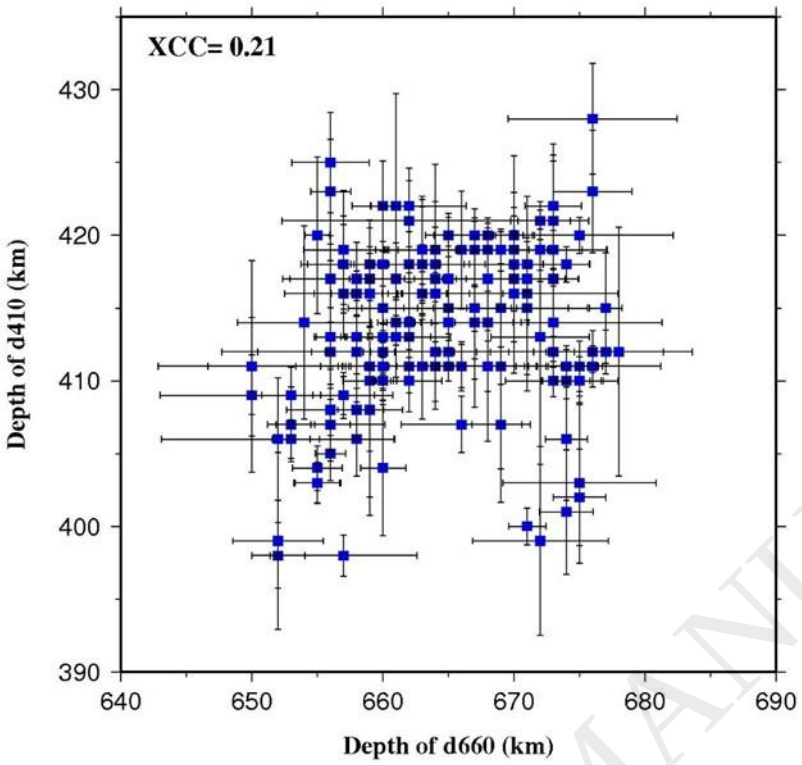

Figr-7

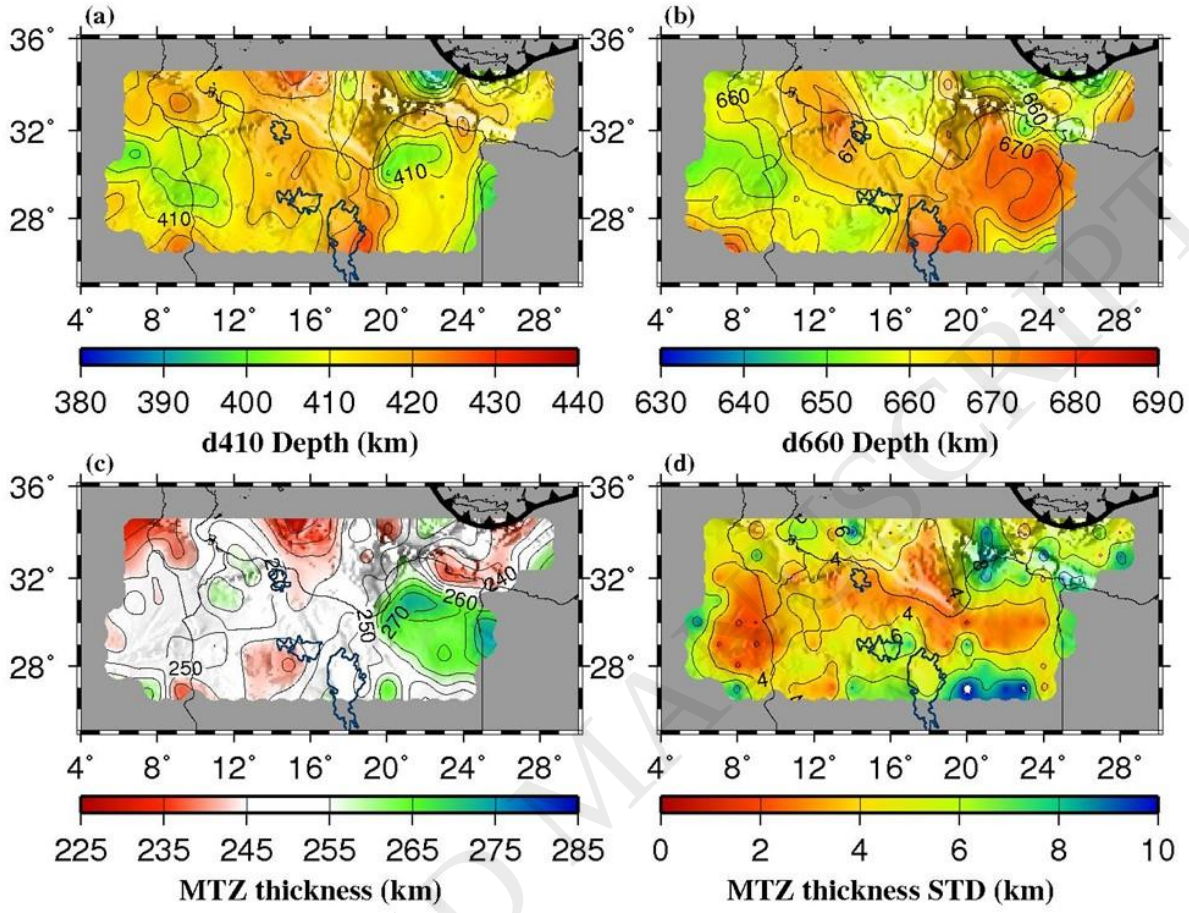

Figr-8

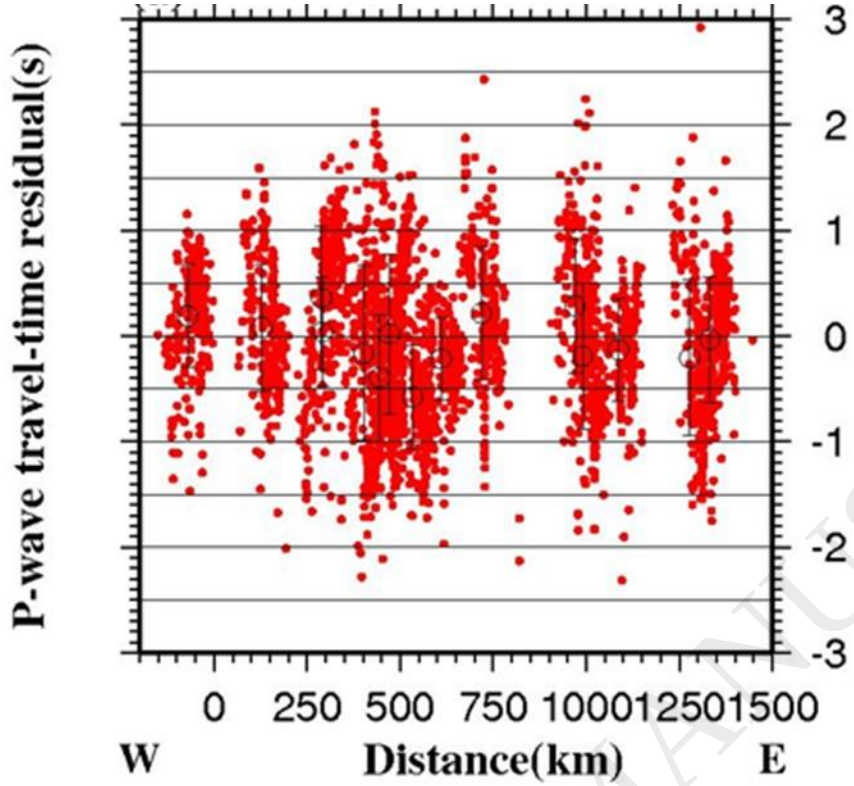

Figr-9